ORIGINAL ARTICLE

GOLD NANOPARTICLES CONJUGATED WITH RITUXIMAB FOR THE TREATMENT OF CHRONIC LYMPHOCYTIC LEUKAEMIA

SANDA BOCA[1,2#], CIPRIAN LUCAN[3#], IOANA FRINC[4#], BOBE PETRUSHEV[5], TIMEA SIMON[1,2], CRISTIAN BERCE[6], GRIGORE-ARISTIDE GAFENCU[7], DELIA DIMA[4], ALINA TANASE[8], SONIA SELICEAN[7], VALENTINA PILECZKI[7,9], LAURA POP[7], VLAD MOISOIU[7], ANCA BUZOIANU[10], ADRIAN FLOREA[11], ALEXANDRU IRIMIE[12,13], SIMION ASTILEAN[1,2], ANCA BOJAN[4,14], IOANA BERINDAN-NEAGOE[7,10], CIPRIAN TOMULEASA[4,7]*

[1]*Nanobiophotonics and Laser Microspectroscopy Center, Interdisciplinary Research Institute in Bio-Nano-Sciences, "Babes-Bolyai" University Cluj-Napoca, Romania*
[2]*Faculty of Physics, "Babes-Bolyai" University, Cluj-Napoca, Romania*
[3]*Department of Medicine, "Iuliu Hatieganu" University of Medicine and Pharmacy, Cluj-Napoca, Romania*
[4]*Department of Haematology, "Ion Chiricuta" Oncology Institute, Cluj-Napoca, Romania*
[5]*Department of Pathology, Emergency County Hospital, Cluj-Napoca, Romania*
[6]*Animal Facility, "Iuliu Hatieganu" University of Medicine and Pharmacy, Cluj-Napoca, Romania*
[7]*Research Center for Functional Genomics and Translational Medicine, "Iuliu Hatieganu" University of Medicine and Pharmacy, Cluj-Napoca, Romania*
[8]*Department of Stem Cell Transplantation, Fundeni Clinical Institute, Bucharest, Romania*
[9]*Department of Experimental Therapeutics, The University of Texas MD Anderson Cancer Center, Houston, TX, USA*
[10]*Department of Pharmacology, "Iuliu Hatieganu" University of Medicine and Pharmacy, Cluj-Napoca, Romania*
[11]*Department of Cell and Molecular Medicine, "Iuliu Hatieganu" University of Medicine and Pharmacy, Cluj-Napoca, Romania*
[12] *Department of Surgical and Gynaecological Oncology, "Ion Chiricuta" Oncology Institute, Cluj-Napoca, Romania*
[13]*Department of Surgery, "Iuliu Hatieganu" University of Medicine and Pharmacy, Cluj-Napoca, Romania*
[14]*Department of Haematology, "Iuliu Hatieganu" University of Medicine and Pharmacy, Cluj-Napoca, Romania*

**corresponding author: ciprian.tomuleasa@umfcluj.ro*
[#]*These authors contributed equally to the current paper, being all three considered co-first authors.*

Manuscript received: May 2016

Abstract

Despite the considerable progress in the chronic lymphocytic leukaemia (CLL) therapy, relapse or progression to a Richter syndrome still appears. Thus, a more targeted therapeutic option is required. This can be achieved by increasing the concentration of the cytostatic drug in the tumour while reducing its systemic toxicity. In the continuous effort toward the development of more efficient therapeutics, in the current study we report rituximab conjugated gold nanoparticles for CLL treatment. The formation of rituximab-nanoconjugates was proved by physico-chemical characterization (UV-Vis spectroscopy, zeta potential and dynamic light scattering) and their intracellular internalization was assessed by dark field and transmission electron microscopy. The therapeutic effect of the newly-designed drugs was investigated by cell counting and MTT assays. Results showed that the effect of our drug-nanocarrier is superior compared to that of the drug alone, data confirmed by state-of-the-art analyses of internalization, cell biology (flow cytometry, apoptosis and autophagy assay), genomics (RT-PCR for MS4A1) and proteomics (confocal microscopy and western blotting for CD20). The present work demonstrates that rituximab nanoconjugates can get an efficient trans-membrane delivery inside CLL cells, being validated as real-potential therapeutics with increased efficacy compared to the drug alone.

Rezumat

În ciuda progreselor semnificative în terapia leucemiei limfatice cronice (LLC), multe dintre cazuri vor recidiva sau vor evolua spre sindrom Richter. Astfel, este necesară dezvoltarea unei noi abordări terapeutice, care poate consta în creșterea concentrației de citostatic în celula malignă și reducerea toxicității sistemice. În prezentul studiu raportăm pentru prima dată conjugarea nanoparticulelor de aur (GNP) cu rituximab, pentru terapia LLC. Bioconjugatul Rituximab-GNP a fost ulterior caracterizat fizic (spectroscopie UV-Vis, potențial zeta și microscopie electronică de transmisie) iar internalizarea a fost demonstrată prin microscopie *dark field* și microscopie electronică. Rezultatele au demonstrat că acest nou *nanocarrier* este superior chimioterapiei clasice, prin tehnici de biologie celulară (citometrie în flux, testul apoptozei și testul autofagiei), tehnici genomice (RT-PCR pentru MS4A1) și tehnici proteomice (microscopie confocală și *western blotting* pentru CD20).

Keywords: chronic lymphocytic leukaemia, gold nanoparticles, rituximab, CD20

Introduction

Chronic lymphocytic leukaemia (CLL) is a monoclonal disorder characterized by a continuous accumulation of malignant lymphocytes. CLL is the most common form of leukaemia found in the Western world, with the proportion of cases diagnosed in early stages (Rai stage 0) having risen from 10% to 50% [1-3]. The affected lymphocytes are of B-cell lineage that carries CD5 in 95% of all cases, while the remaining cases involving T lymphocytes represent a distinct disorder. The onset is insidious and is common for a CLL case to be discovered after a routine blood cell count.

Most B-cell malignancies including CLL express the surface marker CD20, which is absent on otherwise similar appearing T-cell malignancies. CD20 is expressed on all stages of B cell development excepting the first and the last. It is present from late pro-B cells through memory cells, but not on either early pro-B cells or plasma blasts and plasma cells. It is found on B-cell lymphomas, hairy cell leukaemia, B-cell chronic lymphocytic leukaemia, and melanoma cancer stem-like malignant cells [4, 5]. As CD20 is an activated glycosylated phosphoprotein expressed on the surface of all B-cells beginning at the pro-B phase and progressively increasing in concentration until maturity, several targeted therapies that involve its use have been developed. CD20 is the main target of the monoclonal antibodies rituximab, obinutuzumab, ibritumomab tiuxetan, and tositumomab, which are all active agents in the treatment of all B cell lymphomas and leukaemias [6, 7].

The best clinical results have been obtained by rituximab in relapsed CLL [8]. Rituximab destroys B cells and is therefore used to treat diseases which are characterized by excessive numbers of B cells, overactive B cells, or dysfunctional B cells. Usually, chemotherapy is not needed in CLL until the patient will become symptomatic or will have paraclinical evidence of rapid disease progression. A wide variety of chemotherapy regimens may be used, including nucleoside analogues, alkylating agents, apart from the use of curative allogeneic stem cell transplantation. The initial standard therapy for most patients with CLL combines an anti-CD20 antibody with chemotherapy (fludarabine/ cyclophosphamide, bendamustine, or chlorambucil) depending on multiple factors including the physical fitness of the patient. However, patients with very high-risk CLL because of a 17p13 deletion (17p-) with or without mutation of TP53 (17p-/TP53mut) have poor responses to chemo-therapy and require alternative treatment regimens containing B-cell receptor (BCR) signalling pathway inhibitors [9, 10]. Rituximab sticks to one side of B cells, where CD20 is forming a cap and draws proteins over that side. The presence of the cap changes the effectiveness of natural killer (NK) cells in destroying the B cells. When an NK cell latches onto the cap, it has 80 % success rate at killing that cell. In contrast, when the B cell lacks this asymmetric protein cluster, it is killed only 40 % of the time [11].

Despite progress in targeted therapy options for CLL, relapse or progression to a Richter syndrome still appears [12]. Thus, a more focused and targeted therapeutic option is required. This can be achieved by increasing the concentration of a cytostatic drug in the tumour while reducing its' systemic toxicity [13]. Progress in nanotechnology has brought to clinicians attention new ways of treating cancer by involving the use of nanoscale drug delivery on various chemical formulations such as liposomes, polymers, peptides, nanogels or nanoparticles [14, 15]. Among these, gold nano-particles are excellent potential candidates to be used as therapeutic agents in the treatment of CLL due to their unique chemical and optical properties. Specifically, the large surface-to-volume ratio and tailorable surface chemistry of gold nanoparticles are amenable for loading a high amount of the drug on their surface and efficiently by carrying and releasing the drug at the targeted location [16]. The plasmonic response in the visible optical region and the effective light scattering at the plasmon resonance make gold nanoparticles very useful imaging agents by allowing their tracking in real time from the moment of the administration to the delivery at the targeted site. All these properties confined in one single particle give them multiple functionalities and capabilities to be used in cancer chemotherapy, including haematological malignancies.

Specifically related to the design of antibody drug-nanocarriers for the treatment of leukaemia, one recent report demonstrated the loading of rituximab onto lipopolyplex nanoparticles [17]. However, very few reported the use of gold nanoparticles for the design of such a conjugate and fewer gave a detailed description regarding the monitoring of the intracellular localization of such nanoparticle-drug carriers without the aid of contrast agents or marker molecules and the intracellular mechanisms that succeed after such an interaction [18]. As for the therapeutic efficacy, solely one group demonstrated the applicability of drug-nanoconjugates on malignant cells and only in the presence of simultaneous laser irradiation [19].

In the continuous effort toward the development of more efficient therapeutic approaches for the treatment of CLL, in the current paper, we report the successful conjugation of rituximab monoclonal antibody-based drug that targets CD20 to gold nanoparticles (GNPs), their effective trans-membrane delivery inside CLL cells and validation as real-

potential therapeutics with increased efficacy in comparison with the drug alone. Supplementary to the reported studies, we investigated the efficiency of newly-designed drugs by comparing their effects on two different CLL cell lines: malignant lymphocytes CLL-AAT and fibroblast-like cells HS 505. Chemotherapy with rituximab already represents a highly-specific-to-patient therapy for CLL, but by conjugating the drug with gold nanoparticles its' efficacy is enhanced, as shown by our data.

Materials and Methods

Materials

Hydrogen tetrachloroaurate trihydrate ($HAuCl_4 \cdot 3H_2O$, 99.99%), trisodium citrate ($C_6H_5Na_3O_7$) and TWEEN® 20 (polyoxyethylenesorbitan monolaurate – molecular weight (mol wt) ~ 1228) were purchased from Sigma-Aldrich. Rituximab (MabThera®) concentrated perfusable solution 100 mg from Roche was diluted to a stock solution of 1 mg/mL concentration prior to use.

Design of GNPs-rituximab nanocarriers and optical characterization

Citrate capped spherical GNPs were synthesized as a result of the aqueous reduction of $HAuCl_4$ with trisodium citrate, according to the Turkevich-Frens protocol. Nanoparticle conjugation with rituximab was achieved by mixing 500 µL of the purified colloid with rituximab at 0.5 mg/mL final drug concentration and incubated overnight at 4ºC. The conjugated nanoparticles were purified by centrifugation and re-suspended in phosphate buffer saline (PBS). The optical response of the prepared nanoparticles was measured by UV-Vis absorption spectroscopy using a Jasco V-670 UV-Vis-NIR spectrometer. Particle size distribution and zeta potential were measured by a Zetasizer NanoZS90 (Malvern).

Cell culture

The human CLL cell lines HS 505.T and CLL-AAT were purchased from ATCC (USA) and DMSZ (Germany). Cell passage and culture was carried out as previously described [19, 20].

Dark field microscopy

Dark field images were acquired using an inverted Zeiss Axio Observer Z1 microscope. 100 W halogen lamp was focused on the sample using a high numerical immersion condenser (NA = 1.4) and the scattered light was collected by an LD Plan-Neofluar 20X objective (NA = 0.4, Zeiss).

Transmission electron microscopy

Characterization of nanoparticles and nanoparticles inside cells was achieved by transmission electron microscopy (TEM). Slides were prepared for TEM according to the usual protocols [21]. Sections were examined using a JEOL JEM 100CX II transmission electron microscope (Jeol Ltd. Japan) at 100 kV acceleration voltage and magnifications between 3600× and 19000×. The most representative images were photographed on 4489 Kodak electron microscope films (Carestream Health Inc., USA) and scanned using an Imacon Flexitight X5 film scanner (Hasselblad Imacon, Sweden).

Cell proliferation

1.5×10^3 cells were plated in 24-well plates (Day 0), treated with the various drug combinations after 24 hours and counted at days 1, 2, 4, 7, 10 and 14 by using both a haemocytometer and a Leica S80 inverted phase microscope, as well as the Countess Automated Cell Counter (Invitrogen).

MTT assay

Cell survival was assessed using the 3-(4,5-Dimethylthiazol-2-yl)-2,5-diphenyltetrazolium bromide (MTT) assay, as previously described [22, 23]. Cells in monolayer culture were cultivated at sub-confluence before being washed twice with phosphate buffer solution (PBS). Cells were then re-suspended in culture medium with foetal bovine serum (FBS), counted, and plated in 100 µL media at 15×10^3 cells/well in 96-well microliter plates and washed and treated with the cytostatic drugs after 24 hours. GNPs-rituximab were compared with the corresponding conventional drug at identical concentrations. Absorbance of the MTT was measured at 492 nm using a BioTek Synergy.

Statistical analysis

The statistical analysis was performed using R (R Development core team, USA) and GraphPad Prism 5.0 (GraphPad Software INC, CA, USA). The obtained data was first examined for normality of distribution using the Shapiro-Wilk test. The distribution of all the obtained data was Gaussian, thus it was analysed using a parametric test (Two-Way ANOVA with Turkey post-test). The differences were considered significant when $p < 0.05$.

Apoptosis assay by flow cytometry

5×10^5 leukaemia cells treated with either GNPs-rituximab, rituximab alone, GNPs alone or non-treated were cultured in a 96-well plate. Cells were double stained with propidium iodide (PI) and annexin-V (Vybrant Apoptosis Assay Kit, Invitrogen). Early apoptosis was evaluated after 4 hours, whereas late apoptosis after 12 hours. Fluorescence intensity was measured using a flow cytometer (BD FACS Canto II) to assess apoptotic or necrotic cells.

Autophagy assay

Cells were treated as for the apoptosis tests above. After 24 hours, cellular autophagy was evaluated (Autophagy assay kit, Sigma Aldrich) and measured using a proprietary fluorescent autophagosome marker (λ_{ex} = 333 nm/λ_{em} = 518 nm). The reading was carried out at a BioTek Synergy H1 microplate spectrophotometer.

DNA and RNA extraction

Total RNA was isolated using TRIzol reagent (Invitrogen), as previously described [24-26].

Quantitative qRT-PCR (qRT-PCR) for mRNA expression

qRP-PCR was performed to confirm the expression of the MS4A1 gene expression, using TaqMan PCR technology. The RT and PCR reactions were run in 96-well plates. Each run consisted of a sRNA or DNA standard (typically 200 fg to 20 attog) in triplicate, 20 unknown samples in duplicate, 1 "no-RT" well for each duplicate unknown to control for tissue-derived DNA contamination, and a "no template" control well consisting of all of the components of the RT and PCR reaction mixtures except RNA to control for extraneous DNA contamination. For the reverse transcription, the reaction mixture contained 2 µL of extracted cellular RNA, 500 µmol/L of each dNTP, 200 to 300 nmol/L of reverse primer, 1X first-strand buffer, 10 mmol/L DTT and 10 units of Superscript II reverse transcriptase in a volume of 10 µL. The reaction mixture was incubated at 50°C for 30 minutes followed by heat inactivation at 72°C for 10 minutes. RT reactions were run in triplicate for the standards and in duplicate for unknown samples.

For the PCR, following first-strand synthesis, all of the 10 µL RT reaction mixture was used for subsequent PCR amplification by adding 40 µL of PCR master mix to the same wells. Amplification and real-time data acquisition were performed in an ABI Prism 7700 Sequence Detector using the following cycle conditions: initial denaturation at 95°C for 1 minute, followed by 40 cycles of denaturation at 95°C for 12 seconds, and annealing at 60°C for 1 minute. The primers used for *MS4A1* (73 bp), the 5' primer was –GTCTTCACTGGTGG GCC– and the 3' primer was –TAATCTGGACAG CCCCCAA–. Cycle passing threshold (Ct) was recorded and normalized to RNU6B expression. Relative expression was calculated as:

$$2^{Ct\_MS4A1\text{-}Ct\_RNU6B}.$$

PCR reactions were carried out in duplicate.

Western blotting

Cells were lysed in Laemmli sample buffer (Bio-Rad, USA) supplemented with a protease inhibitor complete EDTA-free (Roche). Protein concentration was measured using BCA Protein Assay kit (Pierce, Rockford, Massachusetts, USA). Cell lysates (50 µg) were submitted to electrophoresis on 10 - 20% polyacrylamide gels (Bio-Rad) and transferred to ImmobilonPSQ membranes (Millipore, USA). The membranes were blocked with tris buffered saline (TBS) then incubated with the primary antibody, incubated after washing with horseradish peroxidase (HRP)-conjugated goat anti-rabbit IgG (Calbiochem, USA) and analysed using enhanced chemiluminescence-plus reagent (GE Healthcare, United Kingdom). Densitometry was performed on the western blot images by using the J-Image software (http://rsbweb.nih.gov/ij/).

Confocal microscopy

Both cell lines were seeded on poly-L-lysine–coated chamber slides in culture medium. For immune staining, cells were fixed with 4% paraformaldehyde – 0.5% glutaraldehyde and then were permeabilized with 0.5 mL of 0.2% Triton X-100. After blocking with 10% horse serum, slides were incubated with primary antibody at 4°C overnight, followed by staining with Cy3-labeled anti-rabbit IgG conjugate (Calbiochem, USA). Results were visualized by confocal microscopy using an Olympus FV 1200 Multi Photon Laser Scanning Microscope.

Results and Discussion

Physical-chemical characterization of rituximab-nanoconjugates

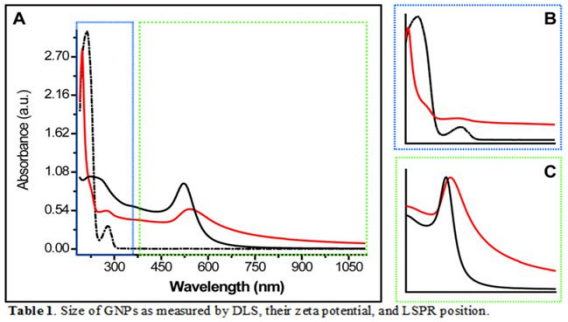

Table 1. Size of GNPs as measured by DLS, their zeta potential, and LSPR position.

Sample	Zeta-potential (mV)	Zeta-deviation (mV)	Diameter (nm)	Polydispersity index (PdI)	LSPR position (nm)
GNPs-TWEEN	-23 ± 0.5	13 ± 1	37 ± 2	0.93	522
GNPs-Rituximab	17± 1	8 ± 1	275± 2	0.21	541

Figure 1.

(A) UV-Vis absorption spectra of the rituximab conjugated nanoparticles in PBS solution (red line), of the same nanoparticles coated by only TWEEN® 20 surfactant, without the drug (black line) and of the free drug in aqueous solution (black, dashed line). (B and C) Magnified, normalized spectra from image (A) represented in the UV (B) and Visible (C) spectroscopic domain.

First characterization of the nanoconjugates was done by measuring the optical spectra of the particles. Figure 1A presents the absorption spectrum of the conjugated nanoparticles in PBS (red line), the spectrum of the nanoparticles coated by only TWEEN® 20 surfactant (black line) and the spectrum of the free drug in aqueous solution (black, dashed line). TWEEN® 20 was used as surface coating for the control nanoparticles due to the presence of its polysorbate 80 analogue excipient in the rituximab drug solution. Spectra analysis (Figure 1C) show a consistent red-shifting of the plasmonic band caused by the refractive index changes of the

surrounding medium which is an indication of drug conjugation on the nanoparticles surface. The spectroscopic signature of the rituximab drug is also present in the GNPs sample after purification (Figure 1B). The surface charge modification of the gold nanoparticles (from -23 mV to +17 mV) represents another demonstration of the efficient drug conjugation (Table in Figure 1). We also investigated the stability of our compound for which we recorded the absorbance spectrum of the particles after several months from the initial conjugation. The results are introduced in Electronic Supplementary file and confirm the high stability of the nanoconjugate after long-term storage.

Evaluation of GNPs-rituximab intracellular internalization

A first biological test was to assess the internalization of the GNP-rituximab complex by the studied cells by dark field microscopy. As gold nanoparticles scatter light strongly at the wave-length of their plasmonic resonance they can be visualized in dark field mode as shiny dots of a specific colour [27]. Multiple, yellow shiny dots can be observed in the dark field images of the samples incubated with nanoparticles (images B and D in Figure 2). As for the white colour dots seen in the control group images (images A and C in Figure 2) they can be attributed to the cancer cell catabolism products [28].

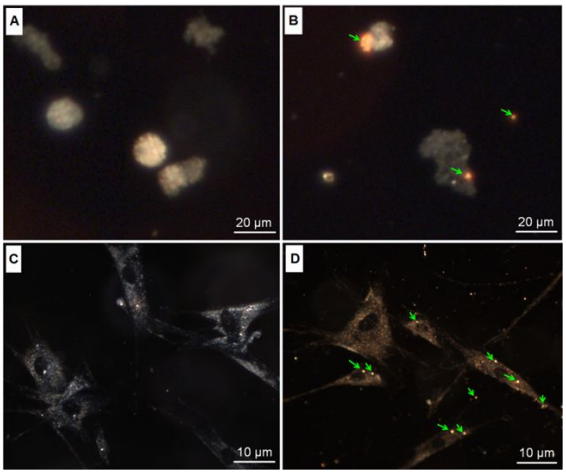

Figure 2.
Dark field microscopy images of CLL-AAT malignant lymphocytes (B) and HS 505. T fibroblast-like cells (D) in the presence of internalized GNPs-rituximab conjugates. Control images of cells without nano-particles are presented in image (A) - CLL-AAT cells and (C) - HS 505. T cells.

For control, each experiment and statement was verified using at least two assays. As such, the dark field microscopy results were corroborated with transmission electron microscopy (TEM). Having a higher accuracy, TEM images demonstrate that the GNPs-rituximab were internalized in the HS 505.T leukaemia cell through the formation of intra-cellular vesicles. Figure 3B depicts such an intracellular vesicle on the inner surface of the cell membrane. Moreover, Figure 3C and 3D illustrate an intracellular vesicle of the malignant lymphocytes CLL-AAT which transports the GNP-rituximab nanostructures throughout the cytoplasm, from the inner cell membrane towards the nuclear membrane. It is curious that the nanoconjugates don't anchor on the inner surface of the cell membrane. A possible explanation for this is given by current data which states that although CD20, the target of rituximab, is a protein trans-membrane protein [29], is also linked to membrane micro-domains known as lipid rafts, enriched in src-family tyrosine kinases and other signalling effectors. This suggests an indirect mechanism of anti-CD20-induced apoptosis in which activation of src-family kinases occurs as a consequence of lipid raft clustering [30]. Furthermore, CD20 is also linked to Bcl-2 pathway, one of the main key regulators of apoptosis [31, 32]. Thus, finding a monoclonal antibody designed to target CD20 inside the cell is to be expected, as lately proved by our data.

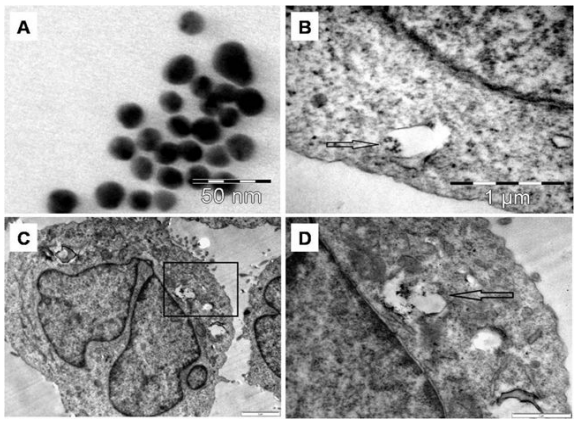

Figure 3.
TEM images for gold nanoparticles, in suspension (A). TEM images for the internalization of the GNP-Rituximab in HS 505. T cells (B) and CLL-AAT cells at different magnifications (C and D).

Assessing the influence of rituximab-nanoconjugates on total cell population

The efficacy of the newly-designed drug-nanocarriers was further tested on the two different CLL cell lines: CLL-AAT and HS 505.T cell lines. CLL-AAT cells were isolated by McWhirter in 2006 from a white male patient [33]. The patient's white blood cell count was 1.6×10^8/mL and > 90% of the CD45+ lymphocyte population expressed Ig D, k light chain, CD5, CD19, and CD23. Immunophenotyping of the cell line showed high expression of CD20, Ig M, k light chain, CD23, CD38, and CD138, moderate expression of CD19

and CD20, and weak expression of Ig D and CD5. HS 505.T cells are fibroblast-like adherent B-lineage CLL cells isolated from a black female patient with CLL and Kaposi's sarcoma. For the reproducibility of the data, the genetic background of the two very different cell lines regarding is very important. The first biological test was proliferation assay. We compared the results obtained between cells cultured without any drug, cells grown in culture media and added GNPs, cells grown in media with added rituximab drug and cells grown in media with GNPs-rituximab conjugate. Cell proliferation was assessed using both MTT and cell counting assay. Figure 4A and 4B show the proliferation of the CLL-AAT cells (Figure 4A) and HS 505.T cells (Figure 4B) at days 1, 2, 4, 7 and 10. The two-way ANOVA analysis tests show a highly significant statistical difference between the cells cultured in the presence of rituximab and the cells cultured with GNPs-rituximab which becomes significant starting with day 7 ($p < 0.01$) (Table I). The data are confirmed for HS 505.T cells. In this case, the statistically significant difference regarding cell proliferation starts with day 4 ($p < 0.05$) being highly significant ($p < 0.01$) at day 7, (Table II). The cell counting assay was confirmed by the MTT proliferation tests. The survival curves for the two lines are illustrated in Figure 4C (CLL-AAT cells) and Figure 4D (HS 505.T cells) and demonstrate that CLL-AAT cells grown in medium supplemented with rituximab and the equivalent cell sample cultured in medium with GNPs-rituximab presents a highly significant difference ($p < 0.01$) starting from day 7 (Table III). The obtained results on the HS 505.T cell line are similar and are illustrated in Table IV.

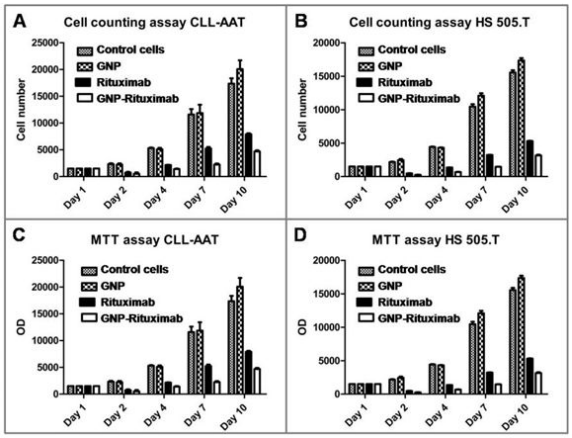

Figure 4.
Cell counting assay for CLL-AAT cells (A) and HS 505. T cells (B) and MTT assay for CLL-ATT cells (C) and HS 505.5 (D).

Table I
Cell counting assay comparing CLL-AAT Rituximab alone *vs.* CLL-AAT GNP-Rituximab

Time	CLL-AAT Rituximab alone	CLL-AAT GNP-Rituximab	Difference	95% CI of diff.
Day 1	1500	1500	0.0000	-1708 to 1708
Day 2	746.7	520.0	-226.7	-1935 to 1481
Day 4	2150	1407	-743.3	-2451 to 964.7
Day 7	5240	2240	-3000	-4708 to -1292
Day 10	7900	4700	-3200	-4908 to -1492

Time	Difference	t	P value	Summary
Day 1	0.0000	0.0000	P > 0.05	ns
Day 2	-226.7	0.4475	P > 0.05	ns
Day 4	-743.3	1.467	P > 0.05	ns
Day 7	-3000	5.922	P<0.001	***
Day 10	-3200	6.317	P<0.001	***

Table II
Cell counting assay comparing HS 505.T rituximab alone *vs.* HS 505.T GNP-Rituximab

Time	HS 505.T Rituximab alone	HS 505.T GNP-Rituximab	Difference	95% CI of diff.
Day 1	1500	1500	0.0000	-806.1 to 806.1
Day 2	473.3	250.3	-223.0	-1029 to 583.1
Day 4	1353	683.3	-670.0	-1476 to 136.1
Day 7	3220	1457	-1763	-2569 to -957.3
Day 10	5310	3153	-2157	-2963 to -1351

Time	Difference	t	P value	Summary
Day 1	0.0000	0.0000	P > 0.05	ns
Day 2	-223.0	0.9328	P > 0.05	ns
Day 4	-670.0	2.803	P < 0.05	*
Day 7	-1763	7.376	P<0.001	***
Day 10	-2157	9.021	P<0.001	***

Table III

Statistical analysis comparing CLL-AAT Rituximab alone *vs.* CLL-AAT GNP-Rituximab

Time	CLL-AAT Rituximab alone	CLL-AAT GNP-Rituximab	Difference	95% CI of diff.
Day 1	1500	1500	0.0000	-1708 to 1708
Day 2	746.7	520.0	-226.7	-1935 to 1481
Day 4	2150	1407	-743.3	-2451 to 964.7
Day 7	5240	2240	-3000	-4708 to -1292
Day 10	7900	4700	-3200	-4908 to -1492

Time	Difference	t	P value	Summary
Day 1	0.0000	0.0000	P > 0.05	ns
Day 2	-226.7	0.4475	P > 0.05	ns
Day 4	-743.3	1.467	P > 0.05	ns
Day 7	-3000	5.922	P<0.001	***
Day 10	-3200	6.317	P<0.001	***

Table IV

Statistical analysis comparing HS 505.T rituximab alone *vs.* HS 505.T GNP-Rituximab

Time	HS 505.T Rituximab alone	HS 505.T GNP-Rituximab	Difference	95% CI of diff.
Day 1	1500	1500	0.0000	-806.1 to 806.1
Day 2	473.3	250.3	-223.0	-1029 to 583.1
Day 4	1353	683.3	-670.0	-1476 to 136.1
Day 7	3220	1457	-1763	-2569 to -957.3
Day 10	5310	3153	-2157	-2963 to -1351

Time	Difference	t	P value	Summary
Day 1	0.0000	0.0000	P > 0.05	ns
Day 2	-223.0	0.9328	P > 0.05	ns
Day 4	-670.0	2.803	P < 0.05	*
Day 7	-1763	7.376	P<0.001	***
Day 10	-2157	9.021	P<0.001	***

Flow cytometry analysis of the leukaemia cells after rituximab-nanoconjugates treatment

Once we have proven that the GNP-rituximab nanoconjugate has an enhanced effect in slowing down leukaemia cell proliferation, we were interested in investigating the cellular mechanisms by which the leukaemia cell is affected by these newly described nanoformulations. Using flow cytometry and Annexin V (AnV) and propidium iodide (PI) staining, we investigated the type of cell death on the leukaemia cells treated with the following combinations: bare GNPs, rituximab drug, and the conjugate GNPs-rituximab. Untreated cells were used as negative controls and H_2O_2 treated necrotic cells were used as positive control.

The initial phase of apoptosis (early apoptosis) involves activation of Bcl-2 family proteins and depolarization of the mitochondria and is a relatively fast process, which happens within hours from the applied stimulus [34]. Later on, changes in nuclear morphology, usually assessed by acridine orange and morphology follow as does cell shrinkage. This was analysed by forward scatter (FS) *versus* side scatter (SS) on flow cytometry. Late apoptosis starts to appear at 5 - 6 hours after the treatment and has a peak at 12 - 16 hours. This happens after caspase activation, nuclear condensation and formation of the apoptotic bodies [35]. If the cell is necrotic, membranes are broken and PI is detected but phosphatidylserine can also be detected, which is usually in the inner side of the membrane except in apoptosis when it translocated to the external site. When membranes are broken in necrosis, PS from the inner site of the membrane can also be detected and you visualize it as An+/PI+. We measured early apoptosis after 4 hours and proved that for both of the cell lines early apoptosis is not the main mechanism of cell death, as seen from Figure 5A-B. The numerical data are presented in Table V and Table VI. The obtained data on late apoptosis measurements conducted after 12 hours from the initial treatment (charts in Figure 5A-B) show that this is the main mechanism of cell death in the case of cells treated with GNP-rituximab complex. However, by our analysis it is observed that a noticeable amount of cells also die due to necrosis but a fine differentiation between those two mechanisms is difficult to establish. This is not of utmost importance, as we have already established that the GNP-rituximab complex kills the leukaemia cell after 12 hours from the administration, which is highly in accordance with the anti-CD20 antibodies mechanisms of action. On the other hand, the autophagy assay showed that autophagy doesn't play any significant role in the death of chronic lymphocytic leukaemia (Figure 5C).

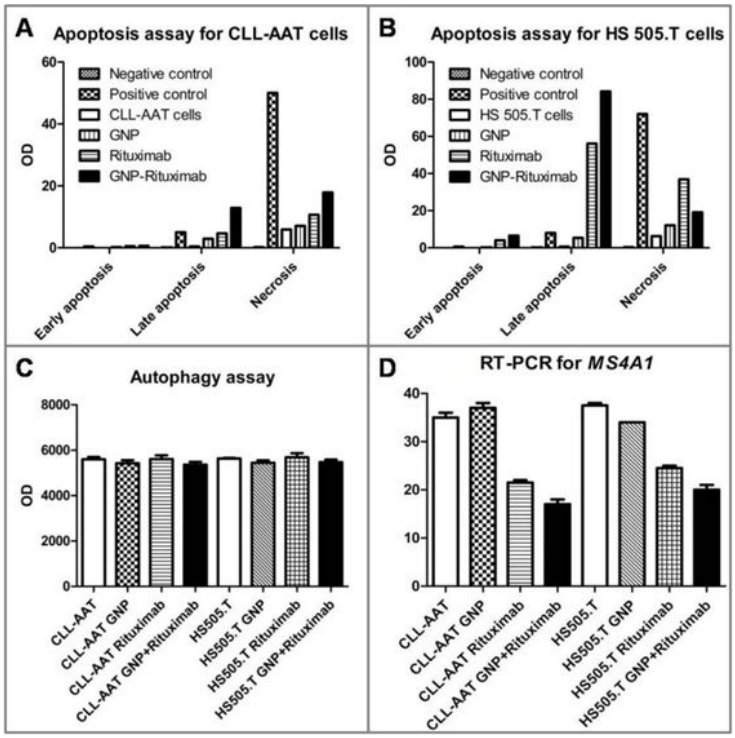

Figure 5.

Apoptosis assay for the investigation of early apoptosis, late apoptosis and necrosis for CLL-AAT cells (A) and HS 505. T cells (B). (C) Autophagy assays for CLL-AAT and HS 505.T cells; (D) RT-PCR analysis for the gene *MS4A1* for CLL-AAT and HS 505.T cells.

Table V

Flow cytometry comparison between the compared samples for early apoptosis, late apoptosis and necrosis

	Negative control	Positive control	CLL-AAT cells	GNP	Rituximab	GNP-Rituximab
Early apoptosis	0	0.4	0	0.2	0.5	0.6
Late apoptosis	0.1	5	0.4	2.9	4.7	12.9
Necrosis	0.2	50	5.9	7.1	10.7	17.9

Table VI

Flow cytometry comparison between the compared samples for early apoptosis, late apoptosis and necrosis

	Negative control	Positive control	HS 505.T cells	GNP	Rituximab	GNP-Rituximab
Early apoptosis	0	0.6	0	0.2	4	6.5
Late apoptosis	0.2	8	0.6	5.4	56.1	84.2
Necrosis	0.4	72	6.3	12.1	36.9	19.1

Genetic analysis of the leukaemia cells after treatment

Up to this point, we demonstrated that the GNP-rituximab bioconjugate has a potential beneficial effect for CLL treatment. Furthermore, we investigated whether rituximab conjugated to gold nanoparticles can act as a targeted therapy against the activated-glycosylated phosphoprotein CD20, the already known target of rituximab. Thus, we measured the anti-CD20 effect of our new drug both at the genetic and genomics and proteomics level. In this regard, we performed a quantitative real time polymerase chain reaction (RT-PCR) for *MS4A1* gene, the gene responsible for the synthesis of the CD20 protein. The membrane-spanning 4-domains, subfamily A, member 1 (*MS4A1*) gene is known to encode the membrane-spanning 4A gene family, characterized by common structural features and very similar intron-exon splice boundaries for hematopoietic cells and non-lymphoid tissues. This gene is involved in the expression of B-lymphocyte surface molecules and is a key gene in the development of B-cells into plasma cells, being localized to 11q22 [4]. The RT-PCR data proved that in the case of cells treated with rituximab, in comparison with the cells which weren't submitted to any treatment, the expression levels of the gene responsible for the synthesis of the CD20 protein is decreased, as seen in Figure 5D. The expression levels is further decreased

when comparing the cells treated with GNPs-rituximab versus the ones treated with rituximab, the difference being statistically significant ($p < 0.01$), as proven using Turkey's Multiple Comparison Test (Table VII).

Table VII

Detailed statistical analysis for cell counting assay

Tukey's Multiple Comparison Test	Mean Diff.	q	Significant? p < 0.05?	Summary	95% CI of diff
CLL-AAT *vs.* CLL-AAT GNP	-2.000	2.596	No	ns	-6.313 to 2.313
CLL-AAT *vs.* CLL-AAT Rituximab	13.50	17.52	Yes	***	9.187 to 17.81
CLL-AAT *vs.* CLL-AAT GNP+Rituximab	18.00	23.36	Yes	***	13.69 to 22.31
CLL-AAT *vs.* HS505.T	-2.500	3.244	No	ns	-6.813 to 1.813
CLL-AAT *vs.* HS505.T GNP	1.000	1.298	No	ns	-3.313 to 5.313
CLL-AAT *vs.* HS505.T Rituximab	10.50	13.63	Yes	***	6.187 to 14.81
CLL-AAT *vs.* HS505.T GNP+Rituximab	15.00	19.47	Yes	***	10.69 to 19.31
CLL-AAT GNP *vs.* CLL-AAT Rituximab	15.50	20.12	Yes	***	11.19 to 19.81
CLL-AAT GNP *vs.* CLL-AAT GNP+Rituximab	20.00	25.96	Yes	***	15.69 to 24.31
CLL-AAT GNP *vs.* HS505.T	-0.5000	0.6489	No	ns	-4.813 to 3.813
CLL-AAT GNP *vs.* HS505.T GNP	3.000	3.893	No	ns	-1.313 to 7.313
CLL-AAT GNP vs HS505.T Rituximab	12.50	16.22	Yes	***	8.187 to 16.81
CLL-AAT GNP *vs.* HS505.T GNP+Rituximab	17.00	22.06	Yes	***	12.69 to 21.31
CLL-AAT Rituximab *vs.* CLL-AAT GNP+Rituximab	4.500	5.840	Yes	*	0.1872 to 8.813
CLL-AAT Rituximab *vs.* HS505.T	-16.00	20.76	Yes	***	-20.31 to -11.69
CLL-AAT Rituximab *vs.* HS505.T GNP	-12.50	16.22	Yes	***	-16.81 to -8.187
CLL-AAT Rituximab *vs.* HS505.T Rituximab	-3.000	3.893	No	ns	-7.313 to 1.313
CLL-AAT Rituximab *vs.* HS505.T GNP+Rituximab	1.500	1.947	No	ns	-2.813 to 5.813
CLL-AAT GNP+Rituximab *vs.* HS505.T	-20.50	26.60	Yes	***	-24.81 to -16.19
CLL-AAT GNP+Rituximab *vs.* HS505.T GNP	-17.00	22.06	Yes	***	-21.31 to -12.69
CLL-AAT GNP+Rituximab *vs.* HS505.T Rituximab	-7.500	9.733	Yes	**	-11.81 to -3.187
CLL-AAT GNP+Rituximab *vs.* HS505.T GNP+Rituximab	-3.000	3.893	No	ns	-7.313 to 1.313
HS505.T *vs.* HS505.T GNP	3.500	4.542	No	ns	-0.8128 to 7.813
HS505.T *vs.* HS505.T Rituximab	13.00	16.87	Yes	***	8.687 to 17.31
HS505.T *vs.* HS505.T GNP+Rituximab	17.50	22.71	Yes	***	13.19 to 21.81
HS505.T GNP *vs.* HS505.T Rituximab	9.500	12.33	Yes	***	5.187 to 13.81
HS505.T GNP *vs.* HS505.T GNP+Rituximab	14.00	18.17	Yes	***	9.687 to 18.31
HS505.T Rituximab *vs.* HS505.T GNP+Rituximab	4.500	5.840	Yes	*	0.1872 to 8.813

Protein analysis of the leukaemia cells after treatment

Once we've shown that the GNPs-rituximab down-regulated the expression of *MS4A1*, the gene responsible for the cellular synthesis of CD20, we were interested in investigating the protein expression by proteomic assays which included western blotting for CD20, as well as confocal microscopy for the same cell membrane protein. Figures 6 and 7 show the protein expression levels for CD20, for the two cell lines, after being treated with the newly synthesized drug. We observe that GNPs-rituximab degrades the protein CD20. In the lower case images the controls for β-actin are presented. Furthermore, confocal microscopy confirmed the qualitative assay of western blotting. The microscopic images of CLL-AAT cells treated with rituximab in Figure 8A show higher quantities of CD20 proteins in comparison with the cells treated with GNPs-rituximab complex (Figure 8B). The same pattern is observed in the case of HS 505.T cells (Figure 8C and Figure 8D).

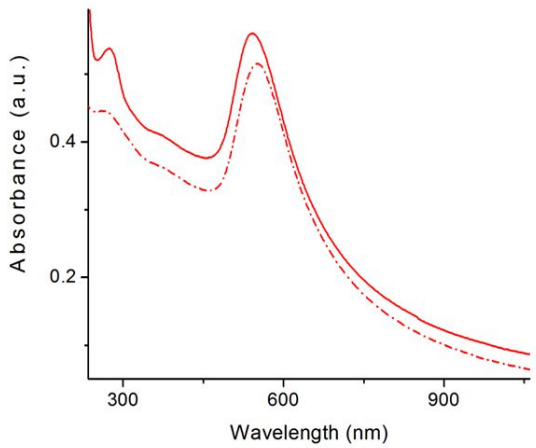

Figure 6.
Zeta potential for the GNP-Rituximab construct

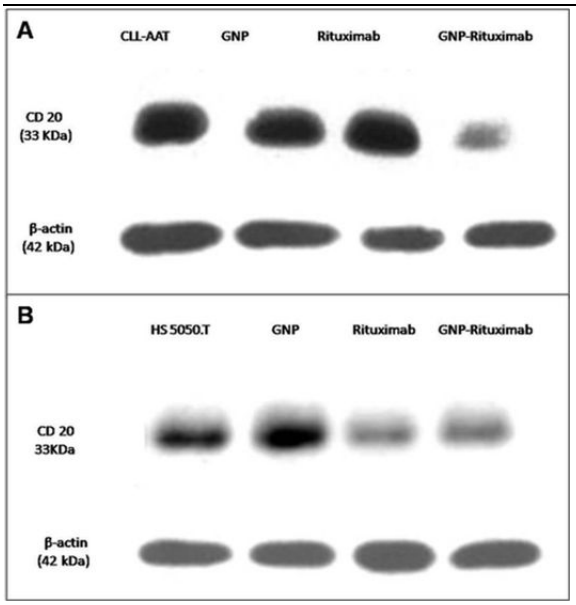

Figure 7.
Western blotting showing the degradation of CD 20, following GNP-Rituximab treatment

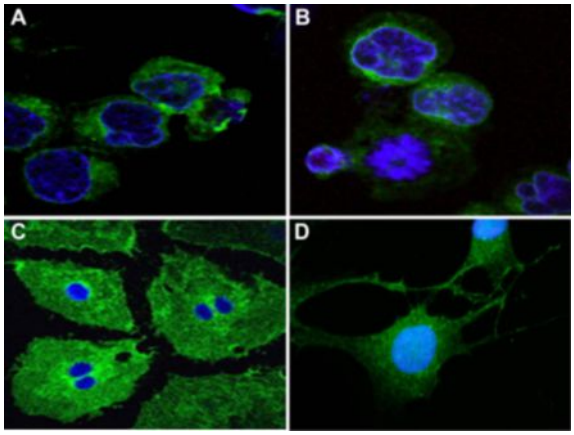

Figure 8.
Confocal microscopy images of CLL-AAT cells treated with rituximab (A) in comparison with the cells treated with GNP-Rituximab (B) confirming of the increased CD20 protein degradation. The same comparison is shown for HS 505.T cells treated with Rituximab (C) *versus* the ones treated with GNP-Rituximab (D).

Conclusions

Herein, we report the design of a new antibody-based drug nanocarrier, its effective trans-membranar delivery and *in vitro* evaluation as therapeutic agent against two different CLL cell lines: malignant lymphocytes CLL-AAT and fibroblast-like cells HS 505.T. The drug-nanocarrier formation was proved by UV-Vis spectroscopy, dynamic light scattering and zeta potential characterization. Nanocarrier cellular internalization was proved by dark field and transmission electron microscopy. The therapeutic effect of the newly-designed nanocarrier was investigated and proved by cell counting and MTT assay. State-of-the-art analyses of internalization, cell biology, genomics and proteomics show that rituximab drug loaded nanoparticles have superior effect in comparison with the drug alone. The obtained results are valuable and promising for validating rituximab-nanocarriers as potential clinical agents for the treatment of chronic lymphocytic leukaemia.

Acknowledgement

This paper is supported by the international grant Romania-European Economical Space (Norway) 2015-2016 (contract 1/25.06.2015). S. Boca acknowledges research grant of the Romanian National Authority for Scientific Research and Innovation, CNCS-UEFISCDI, project number PN-II-RU-TE-2014-4-2426 (NanoMEDLeuKemist).

References

1. Dores G.M., Anderson W.F., Curtis R.E., Landgren O., Ostroumova E., Bluhm E.C., Chronic lymphocytic leukaemia and small lymphocytic lymphoma: overview of the descriptive epidemiology. *Br. J. Haematol.*, 2007; 139(5): 809-819.
2. Tsimberidou A.M., Wen S., McLaughlin P., O'Brien S., Wierda W.G., Lerner S., Other Malignancies in Chronic Lymphocytic Leukemia/Small Lymphocytic Lymphoma. *J. Clin. Oncol.*, 2009; 27(6): 904-910.
3. Wierda W.G., Updates to the Management of Chronic Lymphocytic Leukemia. *J. Natl. Compr. Canc. Netw.*, 2015; 13(5S): 662-665.
4. Tedder T.F., Streuli M., Schlossman S.F., Saito H., Isolation and structure of a cDNA encoding the B1 (CD20) cell-surface antigen of human B lymphocytes. *Proc. Natl. Acad. Sci. U.S.A.*, 1988; 85(1): 208-212.
5. Cragg M.S., Walshe C.A., Ivanov A.O., Glennie M.J., The biology of CD20 and its potential as a target for mAb therapy. *Curr. Dir. Autoimmun.*, 2005; 8: 140-174.
6. Riley J.K., Sliwkowski M.X., CD20: a gene in search of a function. *Semin. Oncol.*, 2000; 27(6 Suppl 12): 17-24.
7. Beers S.A., Chan C.H.T., French R.R., Cragg M.S., Glennie M.J., CD20 as a Target for Therapeutic Type I and II Monoclonal Antibodies. *Semin. Hematol.*, 2010; 47(2): 107-114.
8. Furman R.R., Sharman J.P., Coutre S.E., Cheson B.D., Pagel J.M., Hillmen P., Idelalisib and Rituximab in Relapsed Chronic Lymphocytic Leukemia. *N. Engl. J. Med.*, 2014; 370(11): 997-1007.
9. Stilgenbauer S., Furman R.R., Zent C.S., Management of chronic lymphocytic leukemia. *Am. Soc. Clin. Oncol. Educ. Book ASCO Am. Soc. Clin. Oncol. Meet.*, 2015; 164-175.
10. Bauer K., Rancea M., Roloff V., Elter T., Hallek M., Engert A., Rituximab, ofatumumab and other monoclonal anti-CD20 antibodies for chronic

lymphocytic leukaemia. *Cochrane Database Syst. Rev.*, 2012; 11: CD008079.
11. Rudnicka D., Oszmiana A., Finch D.K., Strickland I., Schofield D.J., Lowe D.C., Rituximab causes a polarization of B cells that augments its therapeutic function in NK-cell-mediated antibody-dependent cellular cytotoxicity. *Blood*, 2013; 121(23): 4694-4702.
12. Fathi A.T., Dec G.W.J., Richter J.M., Chen Y.B., Schwartzenberg S.S., Holmvang G., Case 7-2014. *N. Engl. J. Med.*, 2014; 370(9): 861-872.
13. Berindan-Neagoe I., Braicu C., Craciun L., Irimie A., Takahashi Y., Nanopharmacology in translational hematology and oncology. *Int. J. Nanomedicine*, 2014; 3465.
14. Engin A.B., Neagu M., Golokhvast K., Tsatsakis A., Nanoparticles and endothelium: an update on the toxicological interactions. Farmacia, 2015; 63(6): 792-804.
15. Wolinsky J.B., Colson Y.L., Grinstaff M.W., Local drug delivery strategies for cancer treatment: gels, nanoparticles, polymeric films, rods, and wafers. *J. Control Release Off J. Control Release Soc.*, 2012; 159(1): 14-26.
16. Zharov V.P., Kim J.W., Curiel D.T., Everts M., Self-assembling nanoclusters in living systems: application for integrated photothermal nanodiagnostics and nanotherapy. *Nanomedicine Nanotechnol. Biol. Med.*, 2005; 1(4): 326-345.
17. Yu B., Mao Y., Bai L.Y., Herman S.E.M., Wang X., Ramanunni A., Targeted nanoparticle delivery overcomes off-target immunostimulatory effects of oligonucleotides and improves therapeutic efficacy in chronic lymphocytic leukemia. *Blood*, 2013; 121(1): 136-147.
18. MacLaughlin C.M., Parker E.P.K., Walker G.C., Wang C., Evaluation of SERS labeling of CD20 on CLL cells using optical microscopy and fluorescence flow cytometry. *Nanomedicine Nanotechnol. Biol. Med.*, 2013; 9(1): 55-64.
19. Petrushev B., Tomuleasa C., Soritau O., Aldea M., Pop T., Susman S., Metformin plus PIAF combination chemotherapy for hepatocellular carcinoma. *Exp. Oncol.*, 2012; 34(1): 17-24.
20. Miklášová N., Fischer-Fodor E., Lönnecke P., Tomuleasa C.I., Virag P., Perde Schrepler M., Antiproliferative effect of novel platinum(II) and palladium(II) complexes on hepatic tumor stem cells *in vitro*. *Eur. J. Med. Chem.*, 2012; 49: 41-47.
21. Braicu C., Tomuleasa C., Monroig P., Cucuianu A., Berindan-Neagoe I., Calin G.A., Exosomes as divine messengers: are they the Hermes of modern molecular oncology? *Cell Death Differ.*, 2015; 22(1): 34-45.
22. Tomuleasa C., Soritau O., Brie I., Pall E., Foris V., Dicu T., Mesenchymal stem cell irradiation in culture engages differential effect of hyper-fractionated radiotherapy for head and neck cancers. *J. BUON Off J. Balk. Union. Oncol.*, 2010; 15(2): 348-356.
23. Tomuleasa C., Soritau O., Kacso G., Fischer-Fodor E., Cocis A., Ioani H., Arsenic trioxide sensitizes cancer stem cells to chemoradiotherapy. A new approach in the treatment of inoperable glioblastoma multiforme. *J. BUON Off J. Balk. Union. Oncol.*, 2010; 15(4): 758-762.
24. Peng H., Ishida M., Li L., Saito A., Kamiya A., Hamilton J.P., Pseudogene INTS6P1 regulates its cognate gene INTS6 through competitive binding of miR-17-5p in hepatocellular carcinoma. *Oncotarget.*, 2015; 6(8): 5666-5677.
25. Li L., Zhou L., Li Y., Lin S., Tomuleasa C., MicroRNA-21 stimulates gastric cancer growth and invasion by inhibiting the tumor suppressor effects of programmed cell death protein 4 and phosphatase and tensin homolog. *J. BUON Off J. Balk. Union. Oncol.*, 2014; 19(1): 228-236.
26. Yamanaka S., Olaru A.V., An F., Luvsanjav D., Jin Z., Agarwal R., MicroRNA-21 inhibits Serpini1, a gene with novel tumour suppressive effects in gastric cancer. *Dig. Liver Dis.*, 2012; 44(7): 589-596.
27. Yguerabide J., Yguerabide E.E., Light-scattering submicroscopic particles as highly fluorescent analogs and their use as tracer labels in clinical and biological applications. *Anal. Biochem.*, 1998; 262(2): 157-176.
28. Voiculescu V.M., Popa L.G., Bumbacea, R.S., Nitipir C., Giurcaneanu C., Genetics of psoriasis susceptibility and treatment response. *Farmacia*, 2016; 64(3): 313-322.
29. Maloney D.G., Anti-CD20 Antibody Therapy for B-Cell Lymphomas. *N. Engl. J. Med.*, 2012; 366(21): 2008-2016.
30. Klein C., Lammens A., Schäfer W., Georges G., Schwaiger M., Mössner E., Epitope interactions of monoclonal antibodies targeting CD20 and their relationship to functional properties. *mAbs.*, 2013; 5(1): 22-33.
31. Gupta P., Goldenberg D.M., Rossi E.A., Chang C.H., Multiple signaling pathways induced by hexavalent, monospecific, anti-CD20 and hexavalent, bispecific, anti-CD20/CD22 humanized antibodies correlate with enhanced toxicity to B-cell lymphomas and leukemias. *Blood*, 2010; 116(17): 3258-3267.
32. Berinstein N.L., Buckstein R., Imrie K., Spaner D., Mangel J., Tompkins K., Bcl-2 clearance: optimising outcomes in follicular non-Hodgkin's lymphoma. *Bone Marrow Transplant.*, 2002 Feb; 29(Suppl 1): S14-17.
33. McWhirter J.R., Kretz-Rommel A., Saven A., Maruyama T., Potter K.N., Mockridge C.I., Antibodies selected from combinatorial libraries block a tumor antigen that plays a key role in immunomodulation. *Proc. Natl. Acad. Sci. U.S.A.*, 2006; 103(4): 1041-1046.
34. Sy N., Ms D., Selective Bcl-2 inhibition to treat chronic lymphocytic leukemia and non-Hodgkin lymphoma. *Clin. Adv. Hematol. Oncol. HO.*, 2014; 12(4): 224-229.
35. Darzynkiewicz Z., Bedner E., Traganos F., Murakami T., Critical aspects in the analysis of apoptosis and necrosis. *Hum. Cell.*, 1998 Mar; 11(1): 3-12.